Clinical Proteomics

RESEARCH

Open Access

Plasma-targeted proteomic and lipidomic profiling of MASLD, MASH, and hepatitis C virus infection

Suzumi M. Tokuoka[1], Fumie Hamano[1], Ayako Kobayashi[1], Masaya Sugiyama[2], Hirokazu Takahashi[3], Masashi Mizokami[2] and Yoshiya Oda[1*]

Abstract

Background Metabolic dysfunction-associated steatotic liver disease (MASLD) and metabolic dysfunction-associated steatohepatitis (MASH) are chronic liver diseases characterized by lipid accumulation and persistent inflammation, often progressing to fibrosis or hepatocellular carcinoma (HCC). Hepatitis C virus (HCV) infection shares overlapping pathological features, including chronic inflammation and fibrogenesis. Despite their prevalence, reproducible plasma-level molecular data that capture disease-associated systemic alterations remain limited.

Methods We conducted targeted proteomic and targeted lipidomic profiling of several hundred plasma samples from Japanese patients diagnosed with MASLD, MASH, or HCV infection. Targeted proteomics quantified 184 plasma proteins using the Olink Proximity Extension Assay, and targeted lipidomics quantified approximately 500 phospholipid and triglyceride species using LC/MS-based selected reaction monitoring. Reproducibility was assessed across three independent cohorts.

Results Seven proteins (CASP-8, CCL20, CTSD, SCF, MMP-3, TRAIL, and TWEAK) consistently differed between MASLD and MASH across all cohorts, reflecting coordinated changes related to apoptosis, inflammation, and immune signaling. Similar alterations were observed in HCV (Hepatitis C virus), indicating shared immune dysregulation. Lipidomic analysis revealed reproducible remodeling characterized by decreased ether-linked phosphatidylethanolamine (PE), increased ester-linked PE, and elevated saturated sphingomyelin (SM) in MASH. Correlation analyses indicate coordinated relationships between selected protein and lipid alterations, including relationships between CTSD and PE and triglyceride (TG) species containing linoleic acid (18:2).

Conclusions The results of this research provide value to the field of proteomics as a large-scale, reproducible, and hypothesis-generating plasma dual-omics reference dataset. This study was not designed to establish diagnostic biomarkers, to assess clinical discriminative performance, or to imply causal mechanisms. Instead, by emphasizing reproducibility independent cohorts, we provide a plasma dual-omics reference dataset that captures coordinated immune and lipid metabolic alterations associated with chronic liver disease severity. These data provide a framework and resource for future studies researching risk stratification, therapeutic monitoring, and mechanistic validation in chronic liver disease.

*Correspondence:
Yoshiya Oda
yoda@m.u-tokyo.ac.jp

Full list of author information is available at the end of the article

Keywords Proteomics, Lipidomics, Multi-omics, MASH, MASLD, HCV, Plasma, Clinical samples

Introduction

Two of the most common forms of liver diseases have relatively recently been reclassified : Non-alcoholic fatty liver disease (NAFLD) is now Metabolic Dysfunction-Associated Steatotic Liver Disease (MASLD), and non-alcoholic steatohepatitis (NASH) is now referred to as Metabolic Dysfunction-Associated Steatohepatitis (MASH) [1]. They are characterized by the accumulation of fat and inflammation in the liver, which can often develop into liver fibrosis, cirrhosis, and even hepatocellular carcinoma (HCC) [2]. Therefore, early diagnosis and appropriate therapeutic interventions are crucial. MASLD is closely associated with obesity, type 2 diabetes, dyslipidemia, and other lifestyle-related diseases. The global prevalence of such diseases is estimated at around 25% [3]. Recently, lifestyle-related diseases have garnered attention as important clinical and public health challenges. MASH is a progressive form of MASLD, and requires speedier diagnosis, and more advanced treatment and management [4]. Unfortunately, however, non-invasive biomarkers that more precisely diagnose these diseases and better monitor disease progression and treatment efficacy remain scant [5].

To understand the characteristics of MASLD and MASH, individuals infected with Hepatitis C Virus (HCV) and undergoing treatment were used as the comparison group. HCV infection is recognized as a major chronic liver disease. Both MASLD/MASH and HCV are characterized by chronic inflammation, fibrosis, and increased risk of hepatocarcinogenesis. Therefore, HCV represents an informative comparator for delineating the shared and distinct pathogenic pathways of liver inflammation, fibrosis, and metabolic dysregulation.

Collecting a critical mass of plasma samples from healthy individuals, however, proved impractical because healthy people generally have no particular needs to seek medical help. In addition, rigorously excluding subclinical liver abnormalities in such populations is also challenging. For these reasons, healthy controls were not — or more precisely, could not be — included in this study. Furthermore, biobank-based collections of healthy individuals rarely include matched plasma processing protocols, making them unsuitable for direct molecular comparison with clinical patient cohorts. Accordingly, the present study was designed to compare reproducible molecular patterns across clinically well-characterized chronic liver disease groups using HCV infection as an inflammatory liver disease comparator rather than to define disease-specific diagnostic markers.

Proteomics was selected as an appropriate approach to investigate inflammatory, immune, and fibrotic signaling pathway since only plasma samples were available. Lipidomics was employed to capture the lipid metabolic alterations that are characteristic of chronic liver diseases. Accordingly, proteomic analysis was performed first, followed by lipidomic analysis because proteins influence lipid metabolism and function, and can simplify sample preparation for proteomics.

Our preview work emphasized integrating multi-omics approaches, including proteomics, lipidomics, and metabolomics [6, 7]. However, increased measurement duration and costs, as well as the overwhelming amount of data, has compelled us to employ targeted lipidomics and targeted proteomics in this research. For targeted proteomics, Olink Proteomics' Proximity Extension Assay (PEA) [8] was utilized. Using the Olink Target 96 Series [9] with panels enables quantitative analysis of more than 1,000 proteins in human plasma; however, considering measurement time and costs, we limited our measurements to 184 proteins across 2 panels. Since the progression of MASLD and MASH involves inflammation and damage to the liver [9], not only fat accumulation, we selected the inflammation panel from the Olink Target 96 Series.

Furthermore, since MASLD individuals are commonly associated with metabolic syndrome and have an increased risk of cardiovascular disease, Cardiovascular II and III panels were also candidates. We chose the Cardiovascular III panel to explore new mechanistic insights regarding the relationship between liver disease and cardiovascular outcomes [10] all the more because the panel includes fewer well-defined biomarkers. For targeted lipidomics, we analyzed some 500 types of phospholipids and triglycerides (TGs) using the Selected Reaction Monitoring (SRM) method of Liquid Chromatography/Mass Spectrometry (LC/MS) [7, 11]. The methods we employed provide excellent sensitivity for measuring specific proteins and lipid molecules, ensuring quantitativeness. Dual-omics analysis was chosen as the method of research in order to uncover new knowledge regarding disease mechanisms and related therapeutic targets all the more because of the robust synergy provided by the integration of two different types of omics data. This, in turn, enabled the relationships between liver diseases and proteins or lipids to be assessed. To the best of our knowledge, this research represents the first report of conducting both proteomic and lipidomic analyses at a scale of several hundred plasma samples from Japanese patients diagnosed with chronic liver diseases.

This study focuses on identifying reproducible plasma-level molecular patterns across disease groups, not on

establishing diagnostic thresholds or clinical decision tools.

Experimental section

Demographic characteristics and limitations

Plasma samples from the biobank of the National Center for Global Health and Medicine (197 with MASLD , 81 with MASH and 188 with HCV) and from Saga University Hospital (39 with MASLD and 113 with MASH) were employed in this study. All 618 plasma samples used consisted of three cohorts (Table S1). A liver biopsy was performed to diagnose MASH. Due to the previously-mentioned potential challenges in accurately diagnosing MASH and MASLD, a certain amount of concern that some of the disease specimens employed in this study might include cases with inaccurate diagnoses remained. Detailed clinical information were not uniformly available across all cohorts. Participation was voluntary, and all participants provided signed informed consent forms before registering to participate in this study. An overview of sample allocation for proteomic and lipidomic analyses across the three cohorts is summarized in Table S1. Due to differences in sample availability and analytical feasibility, not all samples were subjected to both proteomic and lipidomic analyses. Due to limitations in plasma volume and the high costs associated with targeted proteomic analyses, not all samples in Cohorts 2 and 3 could be analyzed by both proteomics and lipidomics. Therefore, sample allocation to each analytical platform was determined prior to data acquisition based on predefined criteria. Specifically, targeted proteomics was performed on a subset of samples selected to achieve comparable sample sizes across disease categories while maintaining approximate balance in age and sex distributions.

In contrast, targeted lipidomics was applied to a broader set of samples, as this analysis was less constrained by cost. A small number of samples was subjected only to proteomic analysis due to insufficient remaining plasma volume. Nevertheless, the selection criteria for allocating samples to each analysis were established prior to obtaining the results, and subsequent measurements and analyses were conducted according to these predetermined criteria.

Human plasma samples and quality control sample

This study received approval from the Research Ethics Committee of the Faculty of Medicine of The University of Tokyo (Approval numbers 2019282NI-(2), 2019283NI-(2), and 2019022NI). Ethical approval for this research was obtained from the Ethics Committee of The University of Tokyo Hospital in strict compliance with pertinent university, local, and national guidelines and regulatory standards. To control potential order-dependent systematic errors, the samples from different diagnostic groups were arranged in a dispersed pattern throughout the cohort's measurement sequence. To manage potential long-term drifts in LC-MS sensitivity, a stocked pooled sample consisting of randomly selected 1,000 serum samples was utilized as quality control (QC) samples in the measurement.

Reagents

Acetonitrile, 2-propanol (LC/MS grade), and ammonium formate (Wako special grade) from FUJIFILM Wako Pure Chemical Corp. (Osaka, Japan) were the reagents used. Ultrapure water was prepared using the Milli-Q system (Millipore, Billerica, MA, USA). All reagents for PEA proteomics were obtained from Olink Proteomics (Uppsala, Sweden).

PEA proteomics

CARDIOVASCULAR III and INFLAMMATION panels obtained from Olink Proteomics (Uppsala, Sweden) were used. One μL plasma was used for each panel assay. This experiment utilized the robotic system Maholo equipped with an electronic multi-channel pipette. For the quantification process, the Fluidigm Biomark™ HS system or Olink® Signature Q100 system was used for real-time quantitative polymerase chain reaction (qPCR) analysis. Data was processed with the Olink NPX manager software and transformed to Olink's NPX value, a relative protein quantification unit on a log2 scale. NPX values are derived from threshold cycle (Ct) values obtained through qPCR. No additional batch-wise normalization was applied. Each panel was able to measure 92 proteins, and a total of 184 proteins were measured on two panels. This includes three proteins that were included as measurement targets in both panels. Data for 148 proteins detected from among 184 proteins across all 528 plasma samples in this study were used in the analysis.

Table 1 Proteins with differential levels among clinical categories in MASH and MASLD in Cohort 1

Protein	Uniprot ID	FDR-adjusted BH *p*-value	*p*-value
SCF	P21583	0.0276	0.00036
TWEAK	O43508	0.0276	0.00037
CCL20	Q9NRJ3	0.0324	0.00088
t-PA	P00750	0.0324	0.00094
MMP-3	P08254	0.0324	0.00120
TRAIL	P50591	0.0324	0.00136
CASP-8	Q14790	0.0324	0.00153
CTSD	P07339	0.0419	0.00227

Proteins with FDR-adjusted BH *p*-values of less than 0.05 for Welch's t-test were listed.

Table 2 Proteins with differential levels among clinical categories in Cohort 2

Protein	Uniprot ID	FDR-adjusted BH *p*-value	Tukey's HSD
CASP-8*#	Q14790	3.32E-16	3_MASH-1_HCV; 3_MASH-2_MASLD
t-PA*#	P00750	1.04E-04	2_MASLD-1_HCV; 3_MASH-1_HCV; 3_MASH-2_MASLD
CCL20*#	P78556	1.63E-04	2_MASLD-1_HCV; 3_MASH-2_MASLD
TWEAK*#	O43508	0.00019955	3_MASH-1_HCV; 3_MASH-2_MASLD
CTSD*#	P07339	0.00069465	2_MASLD-1_HCV; 3_MASH-2_MASLD
SCF*#	P21583	0.0011675	2_MASLD-1_HCV; 3_MASH-2_MASLD
TRAIL*#	P50591	0.0015401	3_MASH-1_HCV; 3_MASH-2_MASLD
MMP-3*#	P08254	0.0073831	3_MASH-1_HCV; 3_MASH-2_MASLD
SELE*	P16581	1.32E-11	3_MASH-1_HCV; 3_MASH-2_MASLD
LDL receptor*	P01130	2.29E-09	2_MASLD-1_HCV; 3_MASH-1_HCV; 3_MASH-2_MASLD
MCP-3*	P80098	4.74E-08	3_MASH-1_HCV; 3_MASH-2_MASLD
LAP TGF-beta-1*	P01137	3.19E-07	2_MASLD-1_HCV; 3_MASH-1_HCV; 3_MASH-2_MASLD
HGF*	P14210	4.60E-07	3_MASH-1_HCV; 3_MASH-2_MASLD
FABP4*	P15090	1.42E-06	2_MASLD-1_HCV; 3_MASH-1_HCV; 3_MASH-2_MASLD
CCL16*	O15467	4.36E-06	2_MASLD-1_HCV; 3_MASH-1_HCV; 3_MASH-2_MASLD
ITGB2*	P05107	4.36E-06	3_MASH-1_HCV; 3_MASH-2_MASLD
CASP-3*	P42574	5.90E-06	2_MASLD-1_HCV; 3_MASH-1_HCV; 3_MASH-2_MASLD
IL-1RT2*	P27930	9.88E-06	2_MASLD-1_HCV; 3_MASH-1_HCV; 3_MASH-2_MASLD
IL-12B*	P29460	1.70E-05	2_MASLD-1_HCV; 3_MASH-2_MASLD
GDF-15*	Q99988	2.96E-05	2_MASLD-1_HCV; 3_MASH-2_MASLD
IL7*	P13232	3.10E-05	2_MASLD-1_HCV; 3_MASH-2_MASLD
CDCP1*	Q9H5V8	9.02E-05	2_MASLD-1_HCV; 3_MASH-2_MASLD
PCSK9*	Q8NBP7	1.58E-04	3_MASH-1_HCV; 3_MASH-2_MASLD
RARRES2*	Q99969	1.63E-04	2_MASLD-1_HCV; 3_MASH-1_HCV; 3_MASH-2_MASLD
JAM-A*	Q9Y624	0.0005893	3_MASH-1_HCV; 3_MASH-2_MASLD
TNFRSF9*	Q07011	0.0011404	2_MASLD-1_HCV; 3_MASH-2_MASLD
CD163*	Q86VB7	0.0011675	2_MASLD-1_HCV; 3_MASH-2_MASLD
TIMP4*	Q99727	0.0011675	3_MASH-1_HCV; 3_MASH-2_MASLD
IGFBP-7*	Q16270	0.0015982	2_MASLD-1_HCV; 3_MASH-2_MASLD
ADA*	P00813	0.001641	3_MASH-1_HCV; 3_MASH-2_MASLD
vWF*	P04275	0.0020453	2_MASLD-1_HCV; 3_MASH-2_MASLD
AP-N*	P15144	0.002273	3_MASH-1_HCV; 3_MASH-2_MASLD
TNFRSF14*	Q92956	0.0023743	3_MASH-1_HCV; 3_MASH-2_MASLD
Gal-4*	P56470	0.0041724	3_MASH-2_MASLD
IL-18R1*	Q13478	0.0052014	3_MASH-1_HCV; 3_MASH-2_MASLD
CD40*	P25942	0.0078302	3_MASH-1_HCV; 3_MASH-2_MASLD
CPA1*	P15085	0.008054	3_MASH-1_HCV; 3_MASH-2_MASLD
CTSZ*	Q9UBR2	0.010977	2_MASLD-1_HCV; 3_MASH-2_MASLD
FAS*	P25445	0.011105	3_MASH-2_MASLD
PON3*	Q15166	0.011938	3_MASH-1_HCV; 3_MASH-2_MASLD
ALCAM*	Q13740	0.013208	3_MASH-2_MASLD
CCL11*	P51671	0.013208	3_MASH-1_HCV; 3_MASH-2_MASLD
LTBR*	P36941	0.013626	3_MASH-2_MASLD
CD244*	Q9BZW8	0.020751	2_MASLD-1_HCV; 3_MASH-2_MASLD
TNF-R1*	P19438	0.026383	3_MASH-2_MASLD
CSTB*	P04080	0.028853	3_MASH-1_HCV; 3_MASH-2_MASLD
PLC*	P98160	0.04295	3_MASH-2_MASLD
IGFBP-2	P18065	5.2E-09	2_MASLD-1_HCV; 3_MASH-1_HCV
FGF-21	Q9NSA1	4.74E-08	2_MASLD-1_HCV; 3_MASH-1_HCV
SELP	P16109	0.00000045	2_MASLD-1_HCV; 3_MASH-1_HCV
PAI	P05121	0.00000046	2_MASLD-1_HCV; 3_MASH-1_HCV
GP6	Q9HCN6	0.000014	2_MASLD-1_HCV; 3_MASH-1_HCV
TNFSF14	O43557	0.000014	2_MASLD-1_HCV; 3_MASH-1_HCV

Table 2 (continued)

Protein	Uniprot ID	FDR-adjusted BH *p*-value	Tukey's HSD
CXCL10	P02778	0.0000187	2_MASLD-1_HCV; 3_MASH-1_HCV
OSM	P13725	0.0000902	2_MASLD-1_HCV; 3_MASH-1_HCV
PDGF subunit A	P04085	0.0000922	2_MASLD-1_HCV
CXCL9	Q07325	0.00014097	2_MASLD-1_HCV; 3_MASH-1_HCV
EN-RAGE	P80511	0.00015523	2_MASLD-1_HCV; 3_MASH-1_HCV
CHI3L1	P36222	0.00016305	2_MASLD-1_HCV
IL10	P22301	0.00039744	2_MASLD-1_HCV; 3_MASH-1_HCV
IGFBP-1	P08833	0.00042593	2_MASLD-1_HCV; 3_MASH-1_HCV
IL-18BP	O95998	0.00042593	2_MASLD-1_HCV
STAMBP	O95630	0.00051626	2_MASLD-1_HCV; 3_MASH-1_HCV
TRANCE	O14788	0.00090228	2_MASLD-1_HCV; 3_MASH-1_HCV
CCL19	Q99731	0.0012062	2_MASLD-1_HCV; 3_MASH-1_HCV
CXCL5	P42830	0.0012062	2_MASLD-1_HCV
IL2-RA	P01589	0.0017794	2_MASLD-1_HCV
OPG_c	O00300	0.0028465	2_MASLD-1_HCV; 3_MASH-1_HCV
SLAMF1	Q13291	0.0028689	2_MASLD-1_HCV
AZU1	P20160	0.0035057	2_MASLD-1_HCV; 3_MASH-1_HCV
MMP-9	P14780	0.0046299	2_MASLD-1_HCV
OPG	O00300	0.0057416	2_MASLD-1_HCV; 3_MASH-1_HCV
TLT-2	Q5T2D2	0.0057416	3_MASH-1_HCV
TNFRSF10C	O14798	0.0073831	3_MASH-1_HCV
TGF-alpha	P01135	0.0080214	2_MASLD-1_HCV
CXCL11	O14625	0.011938	2_MASLD-1_HCV
TNFB	P01374	0.011938	2_MASLD-1_HCV
MPO	P05164	0.016457	2_MASLD-1_HCV; 3_MASH-1_HCV
COL1A1	P02452	0.019287	3_MASH-1_HCV
EGFR	P00533	0.019287	2_MASLD-1_HCV
IL-1RT1	P14778	0.025788	2_MASLD-1_HCV
PD-L1	Q9NZQ7	0.026069	2_MASLD-1_HCV
Notch 3	Q9UM47	0.026546	2_MASLD-1_HCV; 3_MASH-1_HCV
CD5	P06127	0.027523	2_MASLD-1_HCV
CD6	P30203	0.027523	2_MASLD-1_HCV
uPA	P00749	0.032758	2_MASLD-1_HCV
AXL	P30530	0.039458	2_MASLD-1_HCV
TFF3	Q07654	0.045234	2_MASLD-1_HCV

Proteins with FDR-adjusted *p*-values of less than 0.05 for the one-way ANOVA test were listed. The symbol # (eight proteins listed at the top of the table; Protein names in bold italics) indicates that the significant MASH–MASLD difference observed in Cohort 1 was replicated in Cohort 2. The asterisk * (39 proteins (Protein names in bold) listed immediately following the #-marked entries indicates significant differences between MASLD and MASH within Cohort 2. Note that some proteins marked with # are also marked with an asterisk *, and in such cases, these proteins are included in the # list at the top. Therefore, the total number of proteins marked with an asterisk * in the table exceeds 39. OPG1 was measured using both panels. Data from the CARDIOVASCULAR III panel for these proteins are indicated by a subscript "_c".

Lipidomics

Measuring phospholipids and TGs was conducted by lipid extraction from plasma by adding 490µl of 2-propanol onto each 10 µL of plasma sample as described previously with minor modifications.[7] The plasma and 2-propanol were mixed with a vortex mixer for 15 seconds at room temperature, and stored at -30°C for one hour. After centrifugation at 10,000 × g for 10 minute, the supernatant was collected and transferred to a 384-well plate for measurements.

For phospholipid measurements, LCMS-8060NX triple quadrupole mass spectrometers equipped with NexeraXS UHPLC (Shimadzu Co., Kyoto, Japan) were used. Shimadzu LabSolutions LCMS software version 5.112 (Shimadzu Co.) was used for instrument operation. Shim-pack Scepter Claris C18-120 columns (2.1 mm × 100 mm, 1.9 µm, Shimadzu Co.) were utilized for reversed-phase chromatography. The flow rate was 0.3 mL/min, and the column temperature was 50 °C. Mobile phase A consisted of 20 mM NH4HCO2/water, and mobile phase B consisted of 20% acetonitrile and 80% 2-propanol (IPA). The pump gradient was programmed as follows: [time (%A/%B), B Curve setting as 0 unless stated]: from 0 min (70/30) to 0.5 min (70/30), to 14.5

Table 3 Proteins with differential levels among clinical categories in Cohort 3

Protein	Uniprot ID	FDR-adjusted BH *p*-value	Tukey's HSD
CASP-8*#	Q14790	4.97E-09	2_MASLD-1_HCV; 3_MASH-1_HCV; 3_MASH-2_MASLD
TWEAK*#	O43508	7.04E-06	3_MASH-1_HCV; 3_MASH-2_MASLD
CTSD*#	P07339	2.34E-05	3_MASH-1_HCV; 3_MASH-2_MASLD
MMP-3*#	P08254	0.0000768	2_MASLD-1_HCV; 3_MASH-1_HCV; 3_MASH-2_MASLD
SCF*#	P21583	7.68E-05	3_MASH-1_HCV; 3_MASH-2_MASLD
TRAIL*#	P50591	0.00035458	3_MASH-1_HCV; 3_MASH-2_MASLD
CCL20*#	P78556	0.0060553	3_MASH-2_MASLD
SELE*	P16581	4.59E-07	2_MASLD-1_HCV; 3_MASH-1_HCV; 3_MASH-2_MASLD
IL7*	P13232	1.58E-06	3_MASH-1_HCV; 3_MASH-2_MASLD
CASP-3*	P42574	2.25E-06	2_MASLD-1_HCV; 3_MASH-1_HCV; 3_MASH-2_MASLD
CXCL5*	P42830	6.90E-05	2_MASLD-1_HCV; 3_MASH-2_MASLD
PDGF subunit A*	P04085	7.68E-05	2_MASLD-1_HCV; 3_MASH-2_MASLD
PON3*	Q15166	7.68E-05	3_MASH-1_HCV; 3_MASH-2_MASLD
CHI3L1*	P36222	0.00011115	2_MASLD-1_HCV; 3_MASH-2_MASLD
MCP-3*	P80098	0.00014742	3_MASH-1_HCV; 3_MASH-2_MASLD
FABP4*	P15090	0.00030143	3_MASH-1_HCV; 3_MASH-2_MASLD
GDF-15*	Q99988	0.00038836	2_MASLD-1_HCV; 3_MASH-2_MASLD
IL-1RT2*	P27930	0.0014993	3_MASH-1_HCV; 3_MASH-2_MASLD
CCL23*	P55773	0.0026187	3_MASH-1_HCV; 3_MASH-2_MASLD
CDCP1*	Q9H5V8	0.0070516	2_MASLD-1_HCV; 3_MASH-2_MASLD
CCL11*	P51671	0.0073257	3_MASH-1_HCV; 3_MASH-2_MASLD
DNER*	Q8NFT8	0.013792	2_MASLD-1_HCV; 3_MASH-2_MASLD
TFPI*	P10646	0.017396	3_MASH-1_HCV; 3_MASH-2_MASLD
ITGB2*	P05107	0.01987	3_MASH-1_HCV; 3_MASH-2_MASLD
MCP-2*	P80075	0.028568	2_MASLD-1_HCV; 3_MASH-2_MASLD
IL6*	P05231	0.039581	3_MASH-1_HCV; 3_MASH-2_MASLD
Gal-4*	P56470	0.043253	3_MASH-2_MASLD
IGFBP-7*	Q16270	0.043253	3_MASH-2_MASLD
IGFBP-2	P18065	4.69E-07	2_MASLD-1_HCV; 3_MASH-1_HCV
TNFSF14	O43557	4.69E-07	2_MASLD-1_HCV; 3_MASH-1_HCV
IGFBP-1	P08833	1.39E-06	2_MASLD-1_HCV; 3_MASH-1_HCV
LDL receptor	P01130	1.63E-06	2_MASLD-1_HCV; 3_MASH-1_HCV
FGF-21	Q9NSA1	1.75E-06	2_MASLD-1_HCV; 3_MASH-1_HCV
OSM	P13725	1.75E-06	2_MASLD-1_HCV; 3_MASH-1_HCV
LAP TGF-beta-1	P01137	7.43E-06	2_MASLD-1_HCV; 3_MASH-1_HCV
SELP	P16109	2.33E-05	2_MASLD-1_HCV; 3_MASH-1_HCV
PAI	P05121	6.60E-05	2_MASLD-1_HCV; 3_MASH-1_HCV
CXCL9	Q07325	0.0000768	2_MASLD-1_HCV; 3_MASH-1_HCV
GP6	Q9HCN6	0.00013729	2_MASLD-1_HCV; 3_MASH-1_HCV
MMP-9	P14780	0.00017729	2_MASLD-1_HCV; 3_MASH-1_HCV
STAMBP	O95630	0.00021226	2_MASLD-1_HCV; 3_MASH-1_HCV
OPG_c	O00300	0.00037758	2_MASLD-1_HCV; 3_MASH-1_HCV
MPO	P05164	0.00060826	2_MASLD-1_HCV; 3_MASH-1_HCV
CCL16	O15467	0.00094184	2_MASLD-1_HCV; 3_MASH-1_HCV
TFF3	Q07654	0.0011618	2_MASLD-1_HCV; 3_MASH-1_HCV
TGF-alpha	P01135	0.0011618	2_MASLD-1_HCV
AZU1	P20160	0.0021148	2_MASLD-1_HCV; 3_MASH-1_HCV
TRANCE	O14788	0.0023726	2_MASLD-1_HCV; 3_MASH-1_HCV
TLT-2	Q5T2D2	0.002569	2_MASLD-1_HCV; 3_MASH-1_HCV
EN-RAGE	P80511	0.0038445	2_MASLD-1_HCV; 3_MASH-1_HCV
OPG	O00300	0.004438	2_MASLD-1_HCV; 3_MASH-1_HCV
IL8	P10145	0.0054583	3_MASH-1_HCV
SCGB3A2	Q96PL1	0.0064909	2_MASLD-1_HCV; 3_MASH-1_HCV

Table 3 (continued)

Protein	Uniprot ID	FDR-adjusted BH *p*-value	Tukey's HSD
Notch 3	Q9UM47	0.013792	2_MASLD-1_HCV; 3_MASH-1_HCV
IL-18BP	O95998	0.015443	2_MASLD-1_HCV
TIMP4	Q99727	0.015443	3_MASH-1_HCV
CPA1	P15085	0.015791	3_MASH-1_HCV
HGF	P14210	0.01765	3_MASH-1_HCV
IFN-gamma	P01579	0.024925	2_MASLD-1_HCV; 3_MASH-1_HCV
CD93	Q9NPY3	0.028568	3_MASH-1_HCV
IL2-RA	P01589	0.028606	2_MASLD-1_HCV
JAM-A	Q9Y624	0.029976	3_MASH-1_HCV
CCL28	Q9NRJ3	0.03836	3_MASH-1_HCV
FGF-19	O95750	0.039581	3_MASH-1_HCV
EGFR	P00533	0.042159	2_MASLD-1_HCV
uPA	P00749	0.047227	2_MASLD-1_HCV

Proteins with FDR-adjusted p-values of less than 0.05 for the one-way ANOVA test were listed. The symbol # (seven proteins listed at the top of the table; Protein names in bold italics) indicates that the significant MASH–MASLD difference observed and replicated across all three cohorts. The asterisk * (21 proteins listed immediately following the # entries; Protein names in bold) indicates significant differences between MASLD and MASH within Cohort 3. Note that some proteins marked with # are also marked with *, and in such cases, these proteins are included in the #-marked list at the top. Therefore, the total number of proteins marked with * in the table exceeds 21. OPG1 was measured using both panels. Data from the CARDIOVASCULAR III panel for these proteins are indicated by a subscript "_c".

min (10/90) with B Curve setting at -3, 14.6 min (3/97), 18.1 min (3/97), 18.2 min (70/30), and 21 min (70/30). The parameters for the mass spectrometer were set as follows: nitrogen gas used as a nebulizer was set at 2.5 L/min, and as a heating gas set at 10 L/min. The drying gas was set at 10 L/min. Argon gas was used for collision-induced dissociation. Interface temperature was 240 °C. Heat block temperature was set at 400 °C, and desolvation line temperature was set at 250 °C. The injection volume was 3 µL. Table S2 shows SRM transitions for phospholipid measurement.

The transition list was developed for phospholipid species that can be measured in human blood samples, based on preliminary experiments. These transitions utilize fragmentation for polar head groups in phospholipids or fragmentation for one of the two fatty acyl chains consisting of the lipids. Transitions that utilize fragmentation characteristics for vinyl ether linkage to fatty chains[12] were also used. To consistently represent the phospholipid species analyzed using these SRM, the following nomenclature was used: peaks were identified using SRM with fragmentation of polar head groups, the phospholipid name is represented by the lipid class, followed by the sum of the carbon atoms in the two fatty chains, and the sum of the double bonds in the two fatty chains (e.g., PC_38:6). For peaks identified using SRM with fragmentation of fatty acyl chains, the phospholipid name is represented by the lipid class and the number of carbon atoms and double bonds of the two fatty acyl chains. Following this, the number of carbon atoms and double bonds of the detected fatty acyl chain were specified (e.g., PC_18:2_20:4_FA_18:2 or PC_18:2_20:4_FA_20:4). In addition, for phospholipids containing one ether-linked chain, only the observed single fatty acyl chain is represented because ether bonds do not typically produce fatty acyl fragments upon fragmentation. When several separated peaks were observed for the same SRM transition, they were named as peak 1, peak 2, and peak 3, in order of increasing retention time.

For TG measurements, we used the previously published LC/MS method with minor modifications [12]. LCMS-8040 triple quadrupole mass spectrometers equipped with Nexera UHPLC (Shimadzu Co.) were used. Shimadzu LabSolutions LCMS software version 5.112 (Shimadzu Co.) was used for instrument operation. Shim-pack Velox C18 (2.1 x 50 mm, 2.7 µm), was utilized for reversed-phase chromatography. The flow rate was 0.4 mL/min, and the column temperature was 45 °C. Mobile phase A consisted of 20 mM NH4HCO2/water, mobile phase B consisted of 100% acetonitrile, and mobile phase C consisted of 100% IPA. The pump gradient was programmed as follows: [time (%A/%B/%C)]: from 0 min (15/15/70) to 0.1 min (15/15/70), to 8.4 min (5/20/75), 9 min (5/20/75), 9.1 min (15/15/70), and 11 min (15/15/70). The parameters for the mass spectrometer were set as follows: nitrogen gas used as a nebulizer was set at 2.5 L/min, and drying gas was set at 10 L/min. Argon gas was used for collision-induced dissociation. Heat block temperature was set at 400 °C, and desolvation line temperature was set at 250 °C. The injection volume was 4 µL. The list for SRM transitions for TGs is shown in Table S3. The transition list was developed for TG species that can be measured in human blood samples based on preliminary experiments, and the SRM transitions detected from all samples were used as result data. In the SRM transitions, Q1 was set as the parent ion of the ammonium adduct, and Q3 was set as the neutral loss of a fatty chain. The species-level TG name

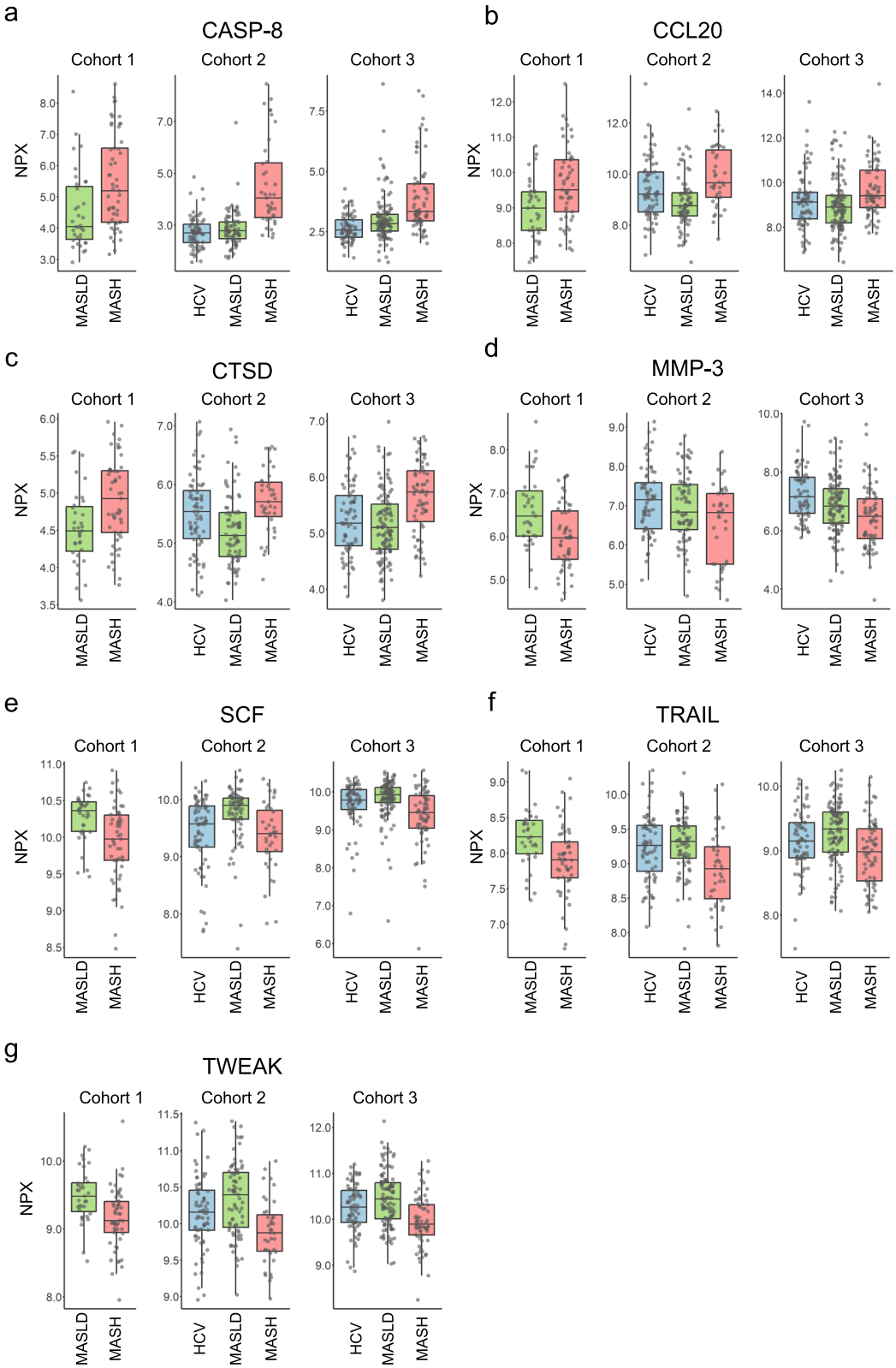

Fig. 1 Proteins with differential levels reproduced in all three Cohorts between MASLD and MASH. Level of proteins CASP-8 (**a**), CCL20 (**b**), CTSD (**c**), MMP-3 (**d**), SCF (**e**), TRAIL (**f**), TWEAK (**g**) in plasma samples in each cohort. The proteins exhibited significant variances by two-tailed Welch's t-test (in Cohort 1) or one-way ANOVA test (in Cohort 2 and Cohort 3) following FDR multiple testing correction and between MASH and MASLD in Tukey's HSD (Honestly Significant Difference) test. Horizontal lines in the rectangles represent the median, boxes represent the interquartile range, and whiskers represent the 5th and 95th percentiles. The dots represent each data point

Table 4 Phospholipids with differential levels reproduced in Cohort 2 and Cohort 3 between MASLD and MASH

Lipid Name	Lipid Class	FDR-adjusted BH *p*-value Cohort 2	FDR-adjusted BH *p*-value Cohort 3	Tukey's HSD Cohort 2	Tukey's HSD Cohort 3
LPC_18:2	PC	3.88E-02	2.07E-02	3_MASH-2_MASLD	2_MASLD-1_HCV; 3_MASH-2_MASLD
LPC_18:2_FA_18:2	PC	3.22E-02	3.12E-02	3_MASH-2_MASLD	3_MASH-2_MASLD
LPC_24:0	PC	1.08E-03	3.60E-02	3_MASH-1_HCV; 3_MASH-2_MASLD	3_MASH-1_HCV; 3_MASH-2_MASLD
PC_18:2_20:4_FA_18:2	PC	1.24E-02	3.37E-02	2_MASLD-1_HCV; 3_MASH-2_MASLD	3_MASH-2_MASLD
PC_33:1	PC	1.89E-02	3.16E-03	2_MASLD-1_HCV; 3_MASH-2_MASLD	2_MASLD-1_HCV; 3_MASH-2_MASLD
PC_36:1	PC	1.08E-03	2.57E-03	3_MASH-1_HCV; 3_MASH-2_MASLD	3_MASH-1_HCV; 3_MASH-2_MASLD
PC_O-34:2_FA_18:2	PC	4.41E-03	3.16E-03	3_MASH-1_HCV; 3_MASH-2_MASLD	3_MASH-1_HCV; 3_MASH-2_MASLD
PC_O-34:2_peak1	PC	1.08E-03	5.47E-03	3_MASH-1_HCV; 3_MASH-2_MASLD	3_MASH-1_HCV; 3_MASH-2_MASLD
PC_O-34:3	PC	2.25E-03	4.20E-04	3_MASH-1_HCV; 3_MASH-2_MASLD	3_MASH-1_HCV; 3_MASH-2_MASLD
PC_O-36:2	PC	3.14E-02	1.84E-02	3_MASH-1_HCV; 3_MASH-2_MASLD	3_MASH-1_HCV; 3_MASH-2_MASLD
PC_O-36:2_FA_18:2	PC	3.15E-02	5.28E-03	3_MASH-1_HCV; 3_MASH-2_MASLD	3_MASH-1_HCV; 3_MASH-2_MASLD
PC_O-36:3	PC	7.44E-03	3.35E-03	3_MASH-1_HCV; 3_MASH-2_MASLD	3_MASH-1_HCV; 3_MASH-2_MASLD
PC_O-38:5	PC	2.33E-02	2.97E-02	3_MASH-1_HCV; 3_MASH-2_MASLD	3_MASH-1_HCV; 3_MASH-2_MASLD
LPE_20:4	PE	4.74E-02	9.62E-03	2_MASLD-1_HCV; 3_MASH-2_MASLD	2_MASLD-1_HCV; 3_MASH-2_MASLD
PE_16:0_22:6_FA_16:0	PE	2.23E-02	1.84E-02	3_MASH-1_HCV; 3_MASH-2_MASLD	3_MASH-1_HCV; 3_MASH-2_MASLD
PE_18:0_22:6_FA_18:0	PE	9.66E-04	4.94E-03	3_MASH-1_HCV; 3_MASH-2_MASLD	3_MASH-1_HCV; 3_MASH-2_MASLD
PE_34:1	PE	3.22E-02	6.87E-03	3_MASH-1_HCV; 3_MASH-2_MASLD	3_MASH-2_MASLD
PE_38:6	PE	2.23E-02	9.91E-03	2_MASLD-1_HCV; 3_MASH-2_MASLD	2_MASLD-1_HCV; 3_MASH-2_MASLD
PE_40:6	PE	3.09E-03	1.09E-02	3_MASH-1_HCV; 3_MASH-2_MASLD	3_MASH-1_HCV; 3_MASH-2_MASLD
PE_O-38:5_FA_22:5	PE	2.34E-02	4.18E-02	3_MASH-2_MASLD	3_MASH-2_MASLD
PE_O-40:6_FA_22:5	PE	4.66E-03	3.16E-03	2_MASLD-1_HCV; 3_MASH-2_MASLD	2_MASLD-1_HCV; 3_MASH-2_MASLD
PE_O-38:6_FA_22:5	PE	9.55E-04	2.57E-03	2_MASLD-1_HCV; 3_MASH-2_MASLD	2_MASLD-1_HCV; 3_MASH-2_MASLD
PE_P-16:0_22:5	PE	4.78E-03	2.57E-03	2_MASLD-1_HCV; 3_MASH-2_MASLD	2_MASLD-1_HCV; 3_MASH-2_MASLD
PE_P-18:0_22:5	PE	1.46E-02	3.16E-03	2_MASLD-1_HCV; 3_MASH-2_MASLD	2_MASLD-1_HCV; 3_MASH-2_MASLD
PE_P-18:1_22:4	PE	2.42E-02	3.16E-02	2_MASLD-1_HCV; 3_MASH-2_MASLD	3_MASH-2_MASLD
PE_P-18:1_22:5	PE	1.24E-02	1.18E-02	2_MASLD-1_HCV; 3_MASH-2_MASLD	2_MASLD-1_HCV; 3_MASH-2_MASLD
SM_36:0;O2	SM	9.55E-04	1.36E-03	3_MASH-1_HCV; 3_MASH-2_MASLD	3_MASH-1_HCV; 3_MASH-2_MASLD
SM_38:0;O2	SM	3.46E-04	8.20E-04	3_MASH-1_HCV; 3_MASH-2_MASLD	3_MASH-1_HCV; 3_MASH-2_MASLD

Phospholipids with an FDR-adjusted *p*-value of less than 0.05 for the one-way ANOVA test and showed significant change with Tukey's HSD post hoc test between MASH and MASLD were listed.

is expressed as the sum of carbon atoms and the sum of double bond equivalents of the three fatty chains. For the TG peaks observed in our SRM analysis, we named them by appending the number of carbon atoms and the number of double bonds of the fatty acyl chain detected as the neutral loss. Peak areas for each SRM were calculated by Traces software [13]. The QC measurements were performed every 12 samples, and raw peak areas were normalized using the systematic error removal by random forest (SERRF) method with the QC measurements [14]. Each normalized SRM peak value was summed for each lipid class, and the individual peak values were then expressed as a ratios to the summed lipid class values.

Statistics

For group comparisons, Welch's t-test ((for two-group comparisons; robust to unequal variances and sample sizes)) and one-way ANOVA (for three-group comparisons) were applied, with p-values adjusted for multiple testing using the Benjamini–Hochberg (BH) false discovery rate (FDR) procedure. Although these tests assume approximate normality, formal normality testing was not used as a primary criterion for feature selection. Given the relatively large sample sizes and the known robustness of t-test and ANOVA to moderate deviations from normality, these parametric tests were applied uniformly across all features. To assess the distributional characteristics of the data, Q–Q plots for features showing consistent differential abundance across cohorts are presented in Figure S1. One-way ANOVA and Welch's t-test (where *p*-values were adjusted for false discovery rate (FDR) using the Benjamini-Hochberg procedure), Pearson's correlation analysis was performed using MetaboAnalyst 6.0 software.[15] Box plots, volcano plots, and scatter plots were constructed using R software (version 4.4.2).

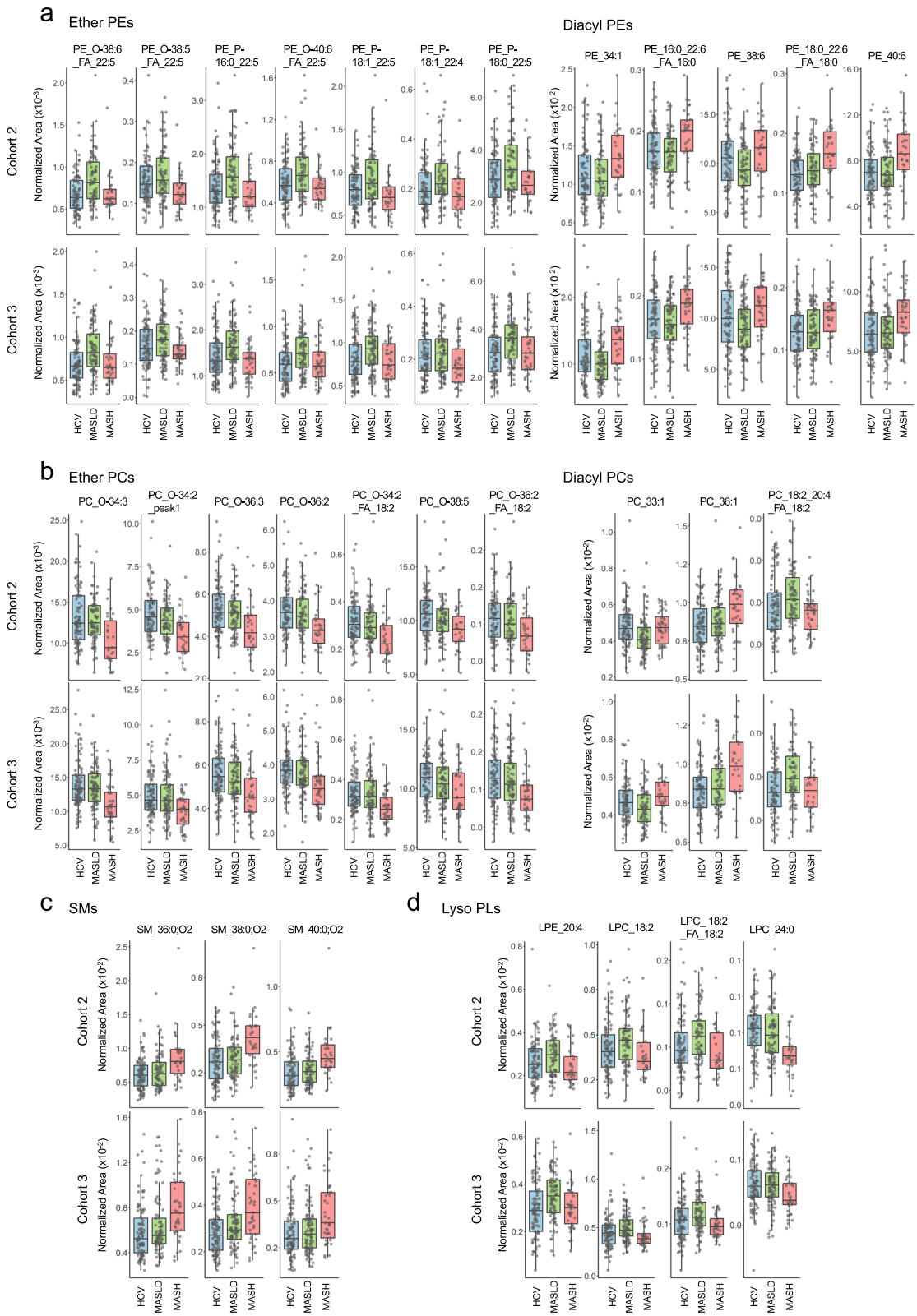

Fig. 2 (See legend on next page.)

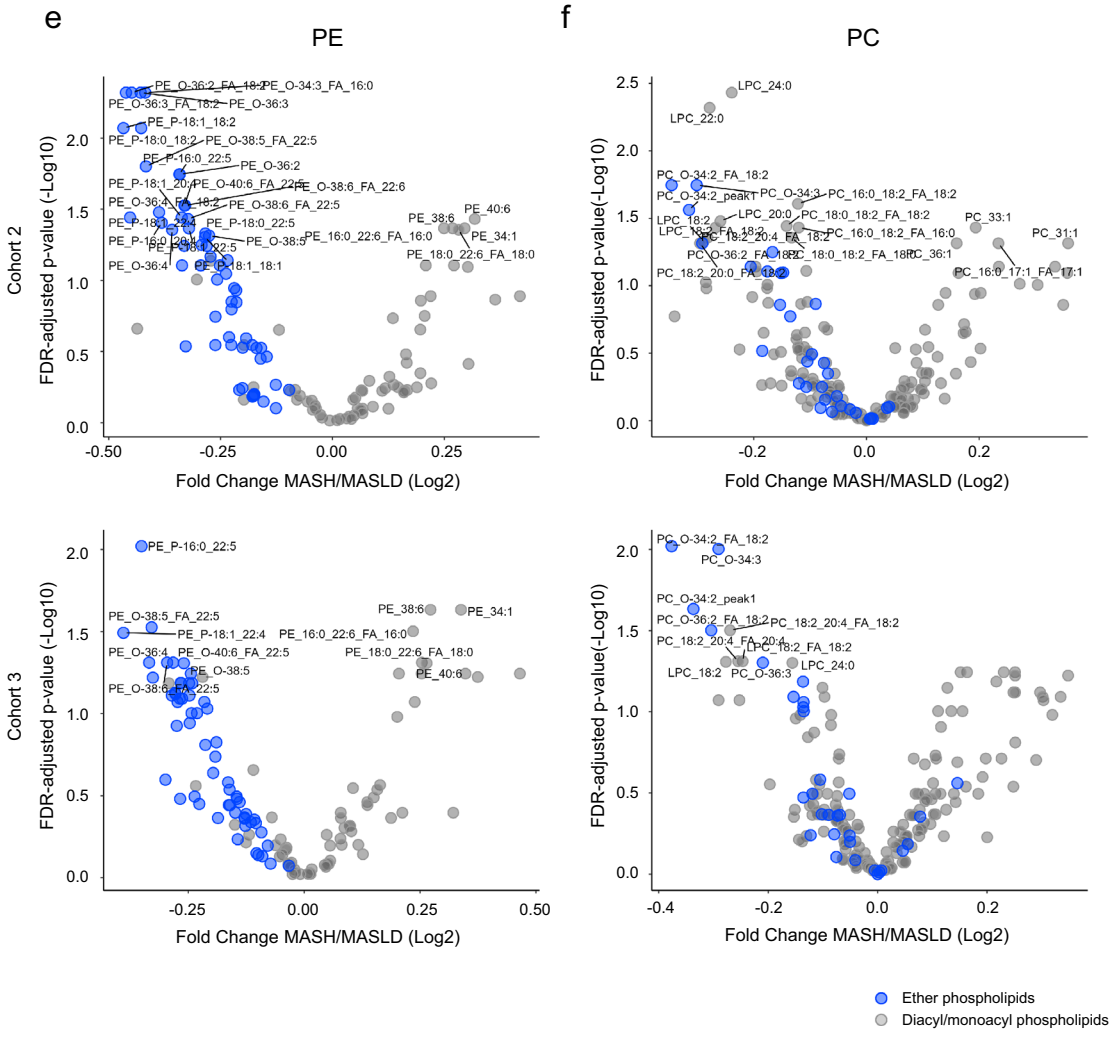

Fig. 2 (continued)

(See figure on previous page.)

Fig. 2 Phospholipids with differential levels between MASLD and MASH. Levels of diradyl PE(**a**), diradyl PC(**b**), SM(**c**), lyso-phospholipid(**d**) are shown. The lipids exhibited significant variances in one-way ANOVA test following FDR multiple testing correction, and between MASH and MASLD in Tukey's HSD test (see Table 4). Horizontal lines in the rectangles represent the median, boxes represent the interquartile range, and whiskers represent the 5th and 95th percentiles. The dots represent each data point. Volcano plots of PE (**e**) and PC (**f**) features are shown. The PE volcano plot includes 123 features, of which 58 are ether species, and the PC volcano plot includes 204 features, of which 32 are ether species. The X-axis represents the log2 fold change between MASH and MASLD. The Y-axis represents the FDR-adjusted p-value by two-tailed Welch's t-test (value of –log10). The blue dots represent ether phospholipids

Results

Targeted proteomics

Targeted proteomics was conducted on plasma samples from 88 individuals (35 with MASLD and 53 with MASH) in Cohort 1, and eight proteins showed significant differences (FDR-adjusted p-values are less than 0.05) between MASLD and MASH (Table 1).

To confirm reproducibility across different samples, targeted proteomics was conducted on plasma samples from 186 individuals (70 with MASLD, 77 with MASH, and 39 with HCV) in Cohort 2, revealing significant differences (FDR-adjusted p-values are less than 0.05) in 88 proteins (Table 2). Among these, 47 proteins marked with an asterisk (*) in Table 2 exhibited significant differences (FDR-adjusted p-values are less than 0.05) between MASLD and MASH, with seven proteins marked with (#) in Table 2 being reproduced in both Cohort 1 and Cohort 2. Seven proteins were proved to be reproducible: CASP-8 (caspase-8), CCL20 (C-C motif chemokine ligand 20), CTSD (cathepsin D), MMP-3 (matrix metalloproteinase-3), SCF (stem cell factor), TRAIL (Tumor Necrosis Factor -related apoptosis-inducing ligand), and TWEAK (Tumor Necrosis Factor-related weak inducer of apoptosis).

Table 5 Phospholipids with differential levels in HCV reproduced in Cohort 2 and Cohort 3

Lipid Name	Lipid Class	FDR-adjusted BH *p*-value Cohort 2	FDR-adjusted BH *p*-value Cohort 3	Tukey's HSD Cohort 2	Tukey's HSD Cohort 3
LPC_22:6	PC	1.24E-02	1.18E-02	2_MASLD-1_HCV; 3_MASH-1_HCV	2_MASLD-1_HCV; 3_MASH-1_HCV
PC_38:3	PC	2.25E-03	1.47E-02	2_MASLD-1_HCV; 3_MASH-1_HCV	2_MASLD-1_HCV; 3_MASH-1_HCV
PC_O-32:1	PC	3.70E-02	1.55E-03	2_MASLD-1_HCV; 3_MASH-1_HCV	2_MASLD-1_HCV; 3_MASH-1_HCV
PC_O-34:1	PC	2.17E-02	9.48E-03	2_MASLD-1_HCV; 3_MASH-1_HCV	2_MASLD-1_HCV; 3_MASH-1_HCV
PC_O-34:2_FA_18:1	PC	1.46E-02	3.16E-03	2_MASLD-1_HCV; 3_MASH-1_HCV	2_MASLD-1_HCV; 3_MASH-1_HCV
PC_O-34:2_peak2	PC	1.46E-02	2.34E-03	2_MASLD-1_HCV; 3_MASH-1_HCV	2_MASLD-1_HCV; 3_MASH-1_HCV
PC_O-36:2_FA_18:1_peak1	PC	3.79E-02	3.16E-03	2_MASLD-1_HCV; 3_MASH-1_HCV	2_MASLD-1_HCV; 3_MASH-1_HCV
PI_18:0_18:2_FA_18:2	PI	2.03E-05	8.20E-04	2_MASLD-1_HCV; 3_MASH-1_HCV	2_MASLD-1_HCV; 3_MASH-1_HCV
PI_36:2	PI	7.92E-05	6.87E-03	2_MASLD-1_HCV; 3_MASH-1_HCV	2_MASLD-1_HCV; 3_MASH-1_HCV
SM_34:0;O2	SM	6.80E-04	6.55E-04	2_MASLD-1_HCV; 3_MASH-1_HCV	2_MASLD-1_HCV; 3_MASH-1_HCV
SM_35:2;O2	SM	2.48E-02	3.83E-03	2_MASLD-1_HCV; 3_MASH-1_HCV	2_MASLD-1_HCV; 3_MASH-1_HCV
SM_36:1;O2	SM	1.50E-06	1.39E-07	2_MASLD-1_HCV; 3_MASH-1_HCV	2_MASLD-1_HCV; 3_MASH-1_HCV
SM_36:2;O2	SM	1.13E-06	1.39E-07	2_MASLD-1_HCV; 3_MASH-1_HCV	2_MASLD-1_HCV; 3_MASH-1_HCV
SM_38:1;O2	SM	1.91E-08	9.26E-08	2_MASLD-1_HCV; 3_MASH-1_HCV	2_MASLD-1_HCV; 3_MASH-1_HCV
SM_40:1;O2	SM	3.77E-07	2.34E-04	2_MASLD-1_HCV; 3_MASH-1_HCV	2_MASLD-1_HCV; 3_MASH-1_HCV
SM_40:2;O2	SM	1.53E-09	1.39E-07	2_MASLD-1_HCV; 3_MASH-1_HCV	2_MASLD-1_HCV; 3_MASH-1_HCV; 3_MASH-2_MASLD
SM_40:3;O2	SM	1.54E-02	5.40E-03	2_MASLD-1_HCV; 3_MASH-1_HCV	2_MASLD-1_HCV; 3_MASH-1_HCV

Phospholipids with an FDR-adjusted *p*-value of less than 0.05 for the one-way ANOVA test and showed significant change with Tukey's HSD post hoc test between HCV and MASLD or HCV and MASH.

Table 6 Triglycerides reproduced in Cohort 2 and Cohort 3 with differential levels between MASLD and MASH

Lipid Name	*p*-value Cohort 2	*p*-value Cohort 3	FDR-adjusted BH *p*-value Cohort 2	FDR-adjusted BH *p*-value Cohort 3	Tukey's HSD Cohort 2	Tukey's HSD Cohort 3	TG Name Species level	Containing fatty chain
TG_50:2-FA_18:1	1.53E-02	2.04E-02	0.0990	0.0999	2_MASLD-1_HCV; 3_MASH-2_MASLD	3_MASH-2_MASLD	TG_50:2	FA_18:1
TG_52:3-FA_16:0	7.41E-03	6.87E-03	0.0956	0.0612	2_MASLD-1_HCV; 3_MASH-2_MASLD	3_MASH-2_MASLD	TG_52:3	FA_16:0
TG_52:3-FA_18:2	1.22E-02	3.63E-03	0.0990	0.0612	3_MASH-2_MASLD	3_MASH-2_MASLD	TG_52:3	FA_18:2
TG_52:4-FA_16:0	7.18E-03	1.41E-03	0.0956	0.0373	3_MASH-2_MASLD	3_MASH-1_HCV; 3_MASH-2_MASLD	TG_52:4	FA_16:0
TG_52:4-FA_18:2	9.05E-03	1.30E-03	0.0956	0.0373	3_MASH-2_MASLD	3_MASH-1_HCV; 3_MASH-2_MASLD	TG_52:4	FA_18:2
TG_52:5-FA_18:2	7.54E-03	3.48E-03	0.0956	0.0612	3_MASH-2_MASLD	3_MASH-1_HCV; 3_MASH-2_MASLD	TG_52:5	FA_18:2
TG_54:5-FA_18:2	4.69E-03	1.38E-03	0.0956	0.0373	3_MASH-1_HCV; 3_MASH-2_MASLD	3_MASH-1_HCV; 3_MASH-2_MASLD	TG_54:5	FA_18:2
TG_54:6-FA_18:2	1.01E-02	1.29E-03	0.0956	0.0373	3_MASH-1_HCV; 3_MASH-2_MASLD	3_MASH-1_HCV; 3_MASH-2_MASLD	TG_54:6	FA_18:2

Triglycerides with FDR-adjusted p-values of less than 0.05 for the one-way ANOVA test and which showed significant change with Tukey`s HSD post hoc test between MASH and MASLD in both Cohort 2 and Cohort 3 were listed

To confirm reproducibility using plasma samples collected from the same 186 individuals as Cohort 2 at different times, we conducted targeted proteomics on 254 plasma samples in Cohort 3 (some individuals had blood drawn twice on different days) (Table 3). The results indicated significant variations in 66 proteins (Table 3), with 28 proteins marked with an asterisk (*) in Table 3 showing significant differences (FDR-adjusted p-values are less than 0.05) between MASLD and MASH. Among these 28 proteins, seven proteins marked with (#) in Table 3 were reproduced across all three cohorts (Fig. 1a-g). Differential abundance analysis of these seven proteins, in addition to the overall proteome-wide patterns, is summarized in the volcano plots for MASLD vs MASH, MASLD vs HCV, and MASH vs HCV (Figure S2).

CASP-8, CCL20, and CTSD were elevated in MASH. MMP-3, SCF, TRAIL, and TWEAK decreased in MASH. Comparing HCV and the other groups, the levels of

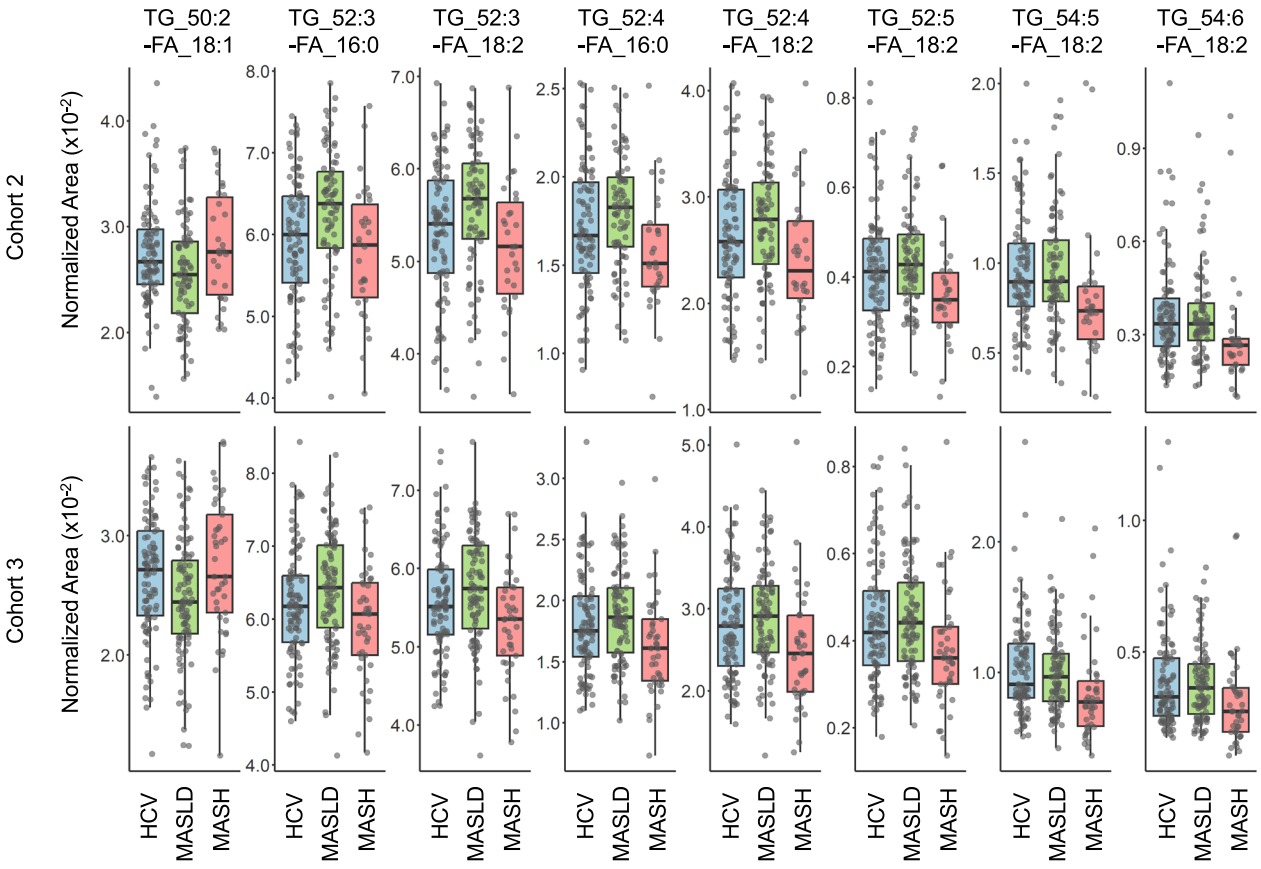

Fig. 3 TGs with differential levels reproduced in Cohort 2 and Cohort 3 between MASLD and MASH. The lipids exhibited significant variances in one-way ANOVA test following FDR multiple testing correction and Tukey's HSD test and between MASH and MASLD (see Table S5-1, Table S5-2, and Table 6). Horizontal lines in the rectangles represent the median, boxes represent the interquartile range, and whiskers represent the 5th and 95th percentiles. The dots represent each data point

CASP-8, MMP-3, TRAIL and TWEAK differed significantly from those in MASH in both Cohort 2 and Cohort 3 (Table 2 and Table 3). Correlation analysis of these seven proteins within all three cohorts revealed that the following pairs showed significant correlations with $p < 0.01$ across all three cohorts: CTSD/CCL20, MMP-3/SCF, MMP-3/TRAIL, MMP-3/TWEAK, SCF/TRAIL, SCF/TWEAK, and TWEAK/TRAIL. The correlation between CASP-8 and CCL20 was somewhat significant only in Cohort 1 at $p = 0.016$, whereas it was significant in Cohort 2 and Cohort 3 ($p < 0.01$) (Table S4, Figure S3). All correlations were positive (Figure S4).

Targeted lipidomics

In Cohort 2 and Cohort 3, targeted phospholipids analysis was performed. The analysis revealed significant differences in 131 phospholipid species in Cohort 2 (Table S5-1) and in 129 phospholipid species in Cohort 3 (Table S5-2), 47 of which showed significant differences between MASLD and MASH in Cohort 2 (Table S5-1) and 49 in Cohort 3 (Table S5-2). Among these, 29 phospholipids demonstrated reproducibility (Table 4). And of these 29 phospholipids, 12 species were identified as diradyl (with two fatty chains) PE, including seven species with an ether bond. Five of these seven species were presumed to have a vinyl-ether bond. Examining the 12 PEs that showed significant alterations in either Cohort 2 or Cohort 3, all seven ether PEs were significantly decreased in MASH compared to MASLD. PEs with two ester bonds, on the other hand, significantly increased in MASH compared to those in MASLD in both Cohort 2 and Cohort 3 (Fig. 2).

All detected PE species are displayed in a volcano plot, and most components with ether bonds were observed to exhibit low values in the MASH (Fig. 2e). Among the 17 phospholipids other than PE, 10 were diradyl phosphatidylcholine (PC), four were lyso PC or lyso PE, and three were saturated sphingomyelin (SM). Similar to PE, ether-linked PC was also found to be lower in MASH (Fig. 2f). The trend of lower and higher levels in ether and diacyl lipids in MASH, however, appears to be more pronounced in PE than in PC. The ether-linked phospholipids for which reproducible changes were observed contained two or more unsaturated bonds. Regarding

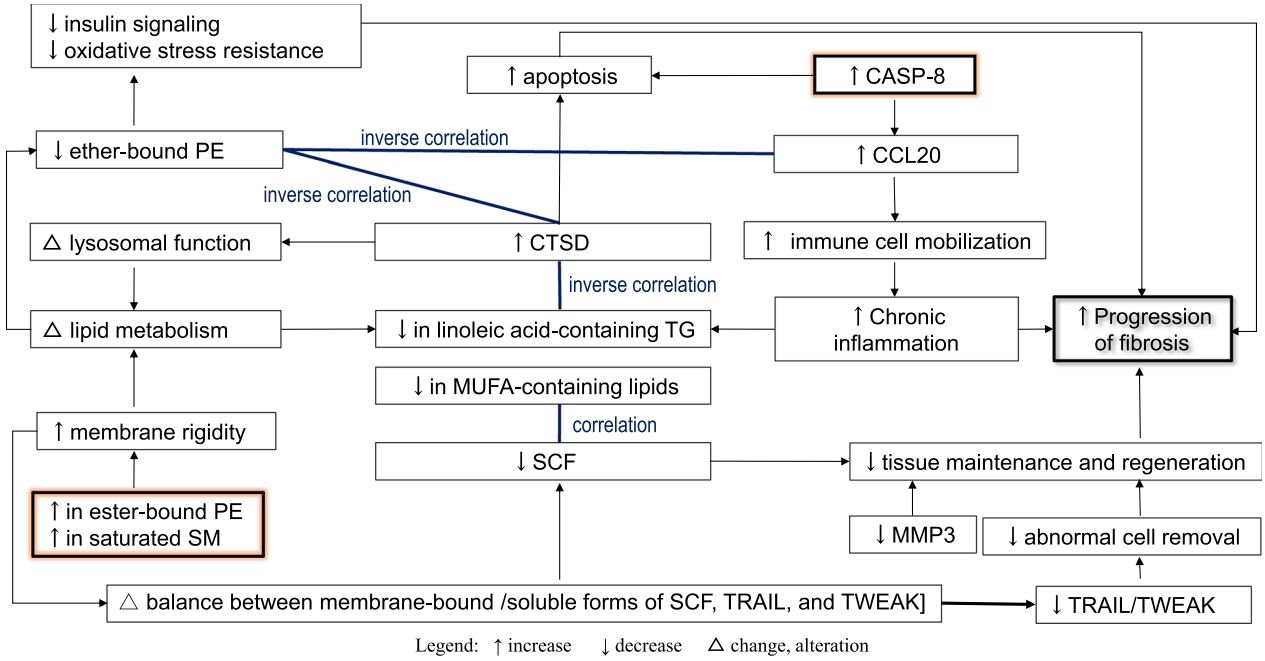

Fig. 4 Relationships between molecules associated with liver inflammation and fibrosis progression. This schematic diagram shows the molecular interactions and correlations between the proteins and lipid species that were the focus of this study. Increased CASP-8 expression promotes apoptosis, leading to elevated CCL20 levels, which in turn enhances immune cell recruitment and chronic inflammation, further accelerates fibrosis progression. Increased levels of ester-linked PE and saturated SM causes elevated membrane rigidity and damaging lipid metabolism. This leads to a decrease in ether-bound PE, which accompanies disrupted insulin signaling, reduced oxidative stress resistance, upregulation of CTSD, and promotion of apoptosis. CTSD expression also accompanies a decrease in linoleic acid-containing TG. Increased membrane rigidity leads to a drop in SCF, to a decrease in MUFA-containing lipids, and to reductions in TRAIL and TWEAK. When combined with a lower level of MMP3, it contributes to the progression of fibrosis by obstructing liver tissue maintenance and abnormal cell removal. The orange boxes indicate the starting points of identifying biomarkers of reactions, the thick black box indicates the final phenotype, and the thick lines indicate significant correlations or inverse correlations. The legend indicates the direction of molecular changes (↑ increase, ↓ decrease, △ alteration)

SMs, three SMs with saturated fatty acids were increased in MASH compared to MASLD (Fig. 2c). The four lyso PLs were all lower in MASH (Fig. 2d). For HCV, 85 phospholipid molecules showed significant differences in both Cohort 2 and Cohort 3 (Observed differences between HCV and MASLD or MASH in both cohorts are indicated by a "†" in Table S5-1 and Table S5-2). Among these, 17 phospholipid molecules exhibited significant differences in both Cohort 2 and Cohort 3 between HCV and MASLD and also between HCV and MASH (Table 5), though no changes were observed for MASLD and MASH (excluding one SM that changed significantly in only one cohort). They included eight SM and six PC components. Since SM has fewer components as targets in this lipidomics research than PC due to the lower variety of SM species in plasma, we conclude that a larger proportion of SMs accounted for the altered lipids in HCV compared to MASH and MASLD (35 targeted features for SMs and 204 targeted features for PCs) (Figure S5).

Next, targeted TG analysis was conducted. In Cohort 2, 26 TG species had an FDR-adjusted p-value smaller than 0.1 (raw p value < 0.02) by ANOVA (Table S6-1), among which 18 TGs marked with an asterisk (*) in Table S6-1 exhibited significant differences between MASLD and MASH. To confirm reproducibility, TG analysis was performed on Cohort 3, and differences in 27 TG species (Table S6-2) were identified. Results showed 14 species indicated with an asterisk (*) in Table S6-2 with differences between MASLD and MASH. Eight TG species marked with ($^{\#}$) in Table S6-1 and Table S6-2 showed proof and reproducible differences between MASLD and MASH across both Cohort 2 and Cohort 3 (Table 6, Fig 3). Of those eight TG molecular species, five contained 18:2 fatty chains. Of note, all five of the 18:2-containing TG components were lower abundance in MASH than in MASLD. The patterns of a low level of 18:2 fatty acyl chain containing TG in MASH were confirmed by a volcano plot of both Cohort 2 and Cohort 3 (Figure S6). To detect characteristics of HCV against MASH or MAFLD, we also listed TG components that differed by ANOVA but not between MASH and MASLD (Table S7, Figure S5).

Correlations for protein-to-lipid interaction between the proteins that showed significant variation across the three cohorts and the lipids that exhibited changes in Cohort 2 and Cohort 3 were analyzed (Table S8, Fig S8). Of the seven proteins (CASP-8, CCL20, CTSD, MMP-3,

SCF, TRAIL, and TWEAK) that showed that the reproducible changes were good between MASLD and MASH. CTSD, in particular, correlated with several PEs: positively with two diacyl PEs and negatively with six ether PEs (Fig S9). In addition, CTSD showed a negative correlation with five TGs containing FA18:2 (Fig S9). Thus, CTSD predominantly correlated with lipids that characterized MASH with lipidomic results. CCL20 also showed a similar trend (one diacyl PE, three ether PEs, two TGs containing FA18:2) although it did not correlate with as many lipids as CTSD. MMP3 was characterized by a negative correlation with PE with FA22:6. For SCF, a negative correlation with lipids having mono-unsaturation was characteristic. Three mono-saturated phospholipids and one TG with mono-saturated fatty acids all showed a negative correlation with SCF (Table S8).

Discussion

Figure 4 summarizes the plasma proteomic and lipidomic plasma associations identified in this study across independent cohorts. CASP-8 is a crucial enzyme for initiating apoptosis via an extrinsic pathway mediated by DR4 and DR5. In MASH, hepatocyte apoptosis increases, and CASP-8 activation contributes to the progression of liver inflammation and fibrosis [16, 17]. Similarly, in HCV infection, cellular stress associated with viral replication activates CASP-8, inducing hepatocyte apoptosis. However, some reports suggest that HCV modulates CASP-8 activity to delay apoptosis and prefers viral persistence, however, this mechanism remains unclear [18].

The chemokine CCL20 recruits CCR6-expressing immune cells, and becomes elevated in MASH liver tissue. This, in turn, intensifies inflammatory responses and immune cell infiltration [19]. In HCV infection, antigen presentation activates immune cells and upregulates CCL20, which further aggravates inflammation. The correlation between CASP-8 and CCL20 expression suggests that apoptotic signals induce CCL20 secretion, exacerbating inflammation even further. Persistent CCL20 elevation in chronic HCV infection likely contributes to excessive immune infiltration and fibrosis, though its mechanistic role is still under investigation [20].

The lysosomal enzyme CTSD is involved in protein degradation and autophagy, and increases as MASLD progresses to MASH, a sign of enhanced cellular stress responses [21]. The significant correlation between CCL20 and CTSD expression suggests that macrophage activation and lysosomal function modulation associated with inflammation are involved. In HCV infection, viral replication alters lysosomal function, potentially modulating CTSD expression and supporting viral persistence, all of which require further investigation. The MMP-3 enzyme is involved in extracellular matrix (ECM) remodeling and decreased in MASH, potentially promoting ECM accumulation and fibrosis [22]. MMP-3 also affects lipid metabolism through adipocyte remodeling and inflammation regulation [23]. The observed reductions in MMP-3, SCF, TRAIL, and TWEAK suggest the presence of damaged liver repair and immune clearance mechanisms that facilitate fibrosis progression.

The growth factor SCF regulates hematopoietic and hepatic stem cells [24–26], and typically increases with early injury or stress, as in MASLD cases where SCF-producing cells decline. As a result, regenerative capacity is diminished. Reduced SCF in a fibrotic, inflammatory environment can prevent liver repair.

The TRAIL protein induces apoptosis by binding to DR4 and DR5 receptors [27]. The protein decreased in MASH, indicating reduced immune clearance of hepatocytes. In HCV infection, TRAIL expression is variable, but can influence hepatocyte injury and clearance [28]. TWEAK protein regulates cell survival, differentiation, and apoptosis via the Fn14 receptor [29]. These levels were elevated in MASH, signifying involvement in hepatocyte injury and fibrosis progression. Both TRAIL and TWEAK are members of the tumor necrosis factor (TNF) superfamily involved in apoptosis regulation [30, 31]. Their concurrent downregulation in MASH suggests a reduction in immune cell-mediated hepatocyte clearance, all of which contribute to chronic inflammation. The significant correlation between TRAIL and TWEAK expression implies a coordinated regulatory mechanism in hepatic immune responses.

In MASH, ether-linked PE O (1-O-alkyl-2-acyl-sn-glycero-3-phosphoethanolamine) and PE P (1-O-(1'Z-alkenyl)-2-acyl-sn-glycero-3-phosphoethanolamine, plasmalogen) are reduced, whereas ester-linked PE increased. These shifts driven by oxidative stress and peroxisomal dysfunction [32], may increase membrane vulnerability to lipid peroxidation [33], promote apoptosis, and destabilize membrane homeostasis [34]. Sphingomyelins (SM) contain saturated fatty acids that rigidify lipid rafts [35]. SMs increased in MASH, which contribute a strong resistance to insulin [36]. Conversely, unsaturated SM (SM_38:2, SM_40:2) is elevated in MASLD, indicating lipid metabolism alterations. On the one hand, the number of TG species containing linoleic acid (18:2) diminished in MASH, likely because of increased β-oxidation or prevented VLDL incorporation. TGs containing DHA or AA, on the other hand, were maintained, likely reflecting their essential structural roles.

The CTSD protein showed a positive correlation with TGs containing linoleic acid, suggesting a role in lipid turnover [37]. In advanced stages of a chronic disease, lysosomal dysfunction may reduce lipid degradation [38], which alters TG homeostasis. SCF correlated inversely with monounsaturated fatty acid (MUFA)-containing lipids across Cohort 2 and Cohort 3, consistent with

compensatory increases in anti-inflammatory MUFAs [39, 40], that attenuate SCF/c-Kit (cluster of differentiation 117) signaling by modifying membrane lipid raft composition [41]. This suggests a lipid-mediated feedback mechanism modulating SCF activity during chronic injury. Although correlations between CCL20 and lipid species were less consistent, inverse associations with ether-type PE and TGs containing linoleic acid were observed in both Cohorts 2 and Cohort 3, suggesting interaction occurs. No reproducible lipid correlations were identified for CASP-8, TRAIL, or TWEAK.

Figure 4 provides a reproducible plasma dual-omics summary that contextualizes coordinated immune and lipid alterations associated with chronic liver disease severity. We do not mean to propose diagnostic biomarkers, predictive models, or clinical decision tools. These reproducible associations may guide future mechanistic and longitudinal research but do not establish causality within the context of this research. Furthermore, this large-scale dual-omics analysis performed exclusively on Japanese patients provides population-specific insights that complement existing data from non-Japanese cohorts, and highlights the need for diverse datasets to advance biomarker discovery and precision medicine in chronic liver diseases.

Conclusions

Our study highlights reproducible plasma molecular features associated with MASH and HCV infection, especially in apoptosis, immune response, and lipid metabolism. CASP-8 activation, together with CCL20, points to apoptotic signals that likely drive immune cell recruitment and chronic inflammation. Lipid alterations in MASH, the reduction of ether-linked PE, and the increase in ester-linked PE and saturated SM all suggest a shift in membrane composition affecting insulin signaling and oxidative stress resistance. Future studies are required to elucidate the metabolic consequences of changes caused by the accumulation of linoleic acid-containing TGs in MASH.

The inverse correlation between CCL20 and ether-linked PE or linoleic acid-containing TGs indicates a potential interaction between immune signaling and lipid metabolism. SCF regulates hematopoietic and hepatic stem cells, and shows a negative relationship with MUFA containing lipids. CTSD, a lysosomal enzyme involved in protein and lipid degradation, inversely correlates with linoleic acid-containing TGs, revealing a potential role in lipid turnover important for regulating body weight and maintaining metabolic health. The roles of CASP-8, TRAIL, and TWEAK in apoptosis and fibrosis are known, and showed no reproducible correlations with lipid species. This suggests that their primary functions in MASH and HCV pathogenesis are likely independent of lipid alterations.

These findings should be regarded as hypothesis-generating and reference-quality, providing reproducible proteomic and lipidomic data from several hundred Japanese patients. The authors would like to stress that this dataset provides a valuable resource for guiding future mechanistic, longitudinal, and translational studies concerning chronic liver disease, and the research is not designed to establish diagnostic biomarkers, to assess clinical discriminative performance, or to infer causal mechanisms.

Abbreviations

BH	Benjamini-hochberg procedure
CASP-8	Caspase-8
CCL20	C-C motif chemokine ligand 20
CTSD	Cathepsin D
ECM	Extracellular matrix
FA	Fatty acid
FDR	False discovery rate
HCC	Hepatocellular carcinoma
HCV	Hepatitis C virus
HSD	Honestly Significant Difference
LC/MS	Liquid chromatography/mass spectrometry
MASH	Metabolic dysfunction-associated steatohepatitis
MASLD	Metabolic dysfunction-associated steatotic liver disease
MMP-3	Matrix metalloproteinase-3
MUFA	Monounsaturated fatty acid
NAFLD	Non-alcoholic fatty liver disease;
NASH	Non-alcoholic steatohepatitis
OPG	Osteoprotegerin
PC	Phosphatidylcholine
PE	Phosphatidylethanolamine
PEA	Proximity extension assay
PL	Phospholipid
QC	Quality control
qPCR	Quantitative polymerase chain reaction
SCF	Stem cell factor
SM	Sphingomyelin
SRM	Selected reaction monitoring
TG	Triglyceride
TNF	Tumor necrosis factor
TRAIL	Tumor necrosis factor-related apoptosis-inducing ligand
TWEAK	Tumor necrosis factor-related weak inducer of apoptosis
VLDL	Very low-density lipoproteins

Supplementary Information

The online version contains supplementary material available at https://doi.org/10.1186/s12014-026-09586-4.

Supplementary Material 1

Supplementary Material 2

Acknowledgments

We would like to express our gratitude to the study participants and all the investigators involved in the study. We are deeply grateful to Dr. Tohru Natsume and members of Robotic Biology Institute Inc. (RBI) for providing us with a humanoid robot Maholo to improve accurate sample handlings. We thank Yoshihiro Kita and Hatsue Igarashi for their assistance. We would like to express our appreciation to Masaki Yamada for his contribution to the creation of our lipidomics methods.

Author contributions

Y.O. conceived and supervised the project and wrote the manuscript. S.M.T. was responsible for lipidomics analyses and preparation of figures and tables.

F.H. and A.K. conducted the proteomics experiments. M.S., H.T., and M.M. were in charge of the collection and storage management of clinical specimens.

Funding
This research was supported by AMED (23tm0624002j0001), AMED (243fa627011h003) and AMED (24ae0121041s0104) (to Y.O.) and JSPS KAKENHI (21K06853) (to S.M.T.). The Department of Lipidomics is supported by the Shimadzu Corporation.

Data availability
The mass spectrometry data have been deposited to Zenodo (Accession Number: https://doi.org/10.5281/zenodo.15728248).

Declarations

Ethics approval
This study received approval from the Research Ethics Committee of the Faculty of Medicine of The University of Tokyo (Approval numbers 2019282NI-(2), 2019283NI-(2), and 2019022NI).

Consent for publication
Not applicable.

Competing interests
The authors declare no competing interests.

Author details
[1]Department of Lipidomics, Graduate School of Medicine, The University of Tokyo, 7-3-1 Hongo, Bunkyo-ku, Tokyo 113-0051, Japan
[2]Department of Viral Pathogenesis and Controls, National Institute of Global Health and Medicine, Japan Institute for Health Security, 1-7-1 Kohnodai, Ichikawa, Chiba 272-8516, Japan
[3]Saga University Hospital, 5-1-1 Nabeshima, Saga 849-8501, Japan

Received: 22 September 2025 / Accepted: 27 January 2026
Published online: 11 February 2026

References

1. Dale K, Fallouh Y, Alkhouri N. MASLD and MASH: how a change of nomenclature may impact our approach in treating liver disease. Expert Opin Investig Drugs. 2024;33(11):1095–7. https://doi.org/10.1080/13543784.2024.2401907.
2. Tacke F, Horn P, Wong VW-S, Ratziu V, Bugianesi E, Francque S, et al. EASL–EASD–EASO clinical practice guidelines on the management of metabolic dysfunction-associated steatotic liver disease (MASLD). J Hepatol. 2024. https://doi.org/10.1016/j.jhep.2024.04.031.
3. Zheng H, Sechi LA, Navarese EP, Casu G, Vidili G. Metabolic dysfunction-associated steatotic liver disease and cardiovascular risk: a comprehensive review. Cardiovasc Diabetol. 2024;23:346. https://doi.org/10.1186/s12933-024-02434-5.
4. Anastasiou G, Stefanakis K, Hill MA, Mantzoros CS. Expanding diagnostic and therapeutic horizons for MASH: comparison of the latest and conventional therapeutic approaches. Metabolism. 2024;161:156044. https://doi.org/10.1016/j.metabol.2024.156044.
5. Yang A, Zhu X, Zhang L, Zhang D, Jin M, Lv G, et al. Evaluating the efficacy of eight non-invasive models in predicting MASLD and progression: a prospective study. BMC Gastroenterol. 2024;24:65. https://doi.org/10.1186/s12876-024-03449-8.
6. Hamano F, Tokuoka SM, Ishibashi M, Yokoi Y, Tourlousse DM, Kita Y, et al. Multi-omics analysis to generate hypotheses for mild health problems in monkeys. Metabolites. 2021;11(10):701. https://doi.org/10.3390/metabo11100701.
7. Tokuoka SM, Hamano F, Kobayashi A, Adachi S, Andou T, et al. Plasma proteomics and lipidomics facilitate elucidation of the link between Alzheimer's disease development and vessel wall fragility. Sci Rep. 2024;14:1–13. https://doi.org/10.1038/s41598-024-71097-9.
8. Wik L, Nordberg N, Broberg J, Björkesten J, Assarsson E, Henriksson S, et al. Proximity extension assay in combination with next-generation sequencing for high-throughput proteome-wide analysis. Mol Cell Proteomics. 2021;20:100168. https://doi.org/10.1016/j.mcpro.2021.100168.
9. Li Y, Yang P, Ye J, Xu Q, Wu J, Wang Y. Updated mechanisms of MASLD pathogenesis. Lipids Health Dis. 2024;23:1. https://doi.org/10.1186/s12944-024-02108-x.
10. Xu S, Zhang G, Tan X, Zeng Y, Jiang H, Jiang Y, et al. Plasma Olink proteomics reveals novel biomarkers for prediction and diagnosis in dilated cardiomyopathy with heart failure. J Proteome Res. 2024;23(9):4139–50. https://doi.org/10.1021/acs.jproteome.4c00522.
11. Anh NK, Thu NQ, Tien NTN, Long NP, Nguyen HT. Advancements in mass spectrometry-based targeted metabolomics and lipidomics: implications for clinical research. Molecules. 2024;29(24):5934. https://doi.org/10.3390/molecules29245934.
12. Zemski Berry KA, Murphy RC. Electrospray ionization tandem mass spectrometry of glycerophosphoethanolamine plasmalogen phospholipids. J Am Soc Mass Spectrom. 2004;15(10):1499–508. https://doi.org/10.1016/j.jasms.2004.07.009.
13. Kita Y, Tokuoka SM, Oda Y, Shimizu T. TRACES: a lightweight browser for liquid chromatography-multiple reaction monitoring-mass spectrometry chromatograms. Metabolites. 2022;12(4):354. https://doi.org/10.3390/metabo12040354.
14. Fan S, Kind T, Cajka T, Hazen SL, Tang WHW, Kaddurah-Daouk R, et al. Systematic error removal using random forest for normalizing large-scale untargeted lipidomics data. Anal Chem. 2019;91(5):3590–6. https://doi.org/10.1021/acs.analchem.8b05592.
15. Pang Z, Lu Y, Zhou G, Hui F, Xu L, Viau C, et al. MetaboAnalyst 6 0: towards a unified platform for metabolomics data processing, analysis and interpretation. Nucleic Acids Res. 2024. https://doi.org/10.1093/nar/gkae253.
16. Orning P, Lien E. Multiple roles of caspase-8 in cell death, inflammation, and innate immunity. J Leukoc Biol. 2021;109(1):121–41. https://doi.org/10.1002/JLB.3MR0420-305R.
17. Wilson CH, Kumar S. Caspases in metabolic disease and their therapeutic potential. Cell Death Differ. 2018;25(5):1010–24. https://doi.org/10.1038/s41418-018-0111-x.
18. Fischer R, Baumert T, Blum HE. Hepatitis C virus infection and apoptosis. World J Gastroenterol. 2007;13(36):4865–72. https://doi.org/10.3748/wjg.v13.i36.4865.
19. Schilcher K, Dayoub R, Kubitza M, Riepl J, Klein K, Buechler C, et al. Saturated fat-mediated upregulation of IL-32 and CCL20 in hepatocytes contributes to higher expression of these fibrosis-driving molecules in MASLD. Int J Mol Sci. 2023;24(17):13222. https://doi.org/10.3390/ijms241713222.
20. Fahey S, Dempsey E, Long A. The role of chemokines in acute and chronic hepatitis C infection. Cell Mol Immunol. 2014;11(1):25–40. https://doi.org/10.1038/cmi.2013.37.
21. Yadati T, Houben T, Bitorina A, Oligschlaeger Y, Gijbels MJ, Mohren R, et al. Inhibition of extracellular cathepsin D reduces hepatic lipid accumulation and leads to mild changes in inflammation in NASH mice. Front Immunol. 2021;12:675535. https://doi.org/10.3389/fimmu.2021.675535.
22. Wan J, Zhang G, Li X, Qiu X, Ouyang J, et al. Matrix metalloproteinase 3: a promoting and destabilizing factor in the pathogenesis of disease and cell differentiation. Front Physiol. 2021;12:663978. https://doi.org/10.3389/fphys.2021.663978.
23. Wu Y, Lee MJ, Ido Y, Fried SK. High-fat diet-induced obesity regulates MMP3 to modulate depot- and sex-dependent adipose expansion in C57BL/6J mice. Am J Physiol Endocrinol Metab. 2017. https://doi.org/10.1152/ajpendo.00128.2016.
24. Mansuroglu T, Ramadori P, Dudás J, Malik I, Hammerich K, et al. Expression of stem cell factor and its receptor c-Kit during the development of intrahepatic cholangiocarcinoma. Lab Invest. 2009;89(5):562–74. https://doi.org/10.1038/labinvest.2009.15.
25. Hu B, Colletti LM. Stem cell factor and c-kit are involved in hepatic recovery after acetaminophen-induced liver injury in mice. Am J Physiol Gastrointest Liver Physiol. 2008. https://doi.org/10.1152/ajpgi.00024.2008.
26. Radmanić L, Zidovec-Lepej S. The role of stem cell factor, epidermal growth factor and angiopoietin-2 in HBV, HCV, HCC and NAFLD. Life. 2022;12(12):2072. https://doi.org/10.3390/life12122072.
27. Schneider P, Thome M, Burns K, Bodmer JL, Hofmann K, Kataoka T, et al. TRAIL receptors 1 (DR4) and 2 (DR5) signal FADD-dependent apoptosis and activate NF-κB. Immunity. 1997;7(6):831–6. https://doi.org/10.1016/S1074-7613(00)80401-X.
28. Rosen HR, Golden-Mason L. Control of HCV infection by natural killer cells and macrophages. Cold Spring Harb Perspect Med. 2020;10(9):a037101. https://doi.org/10.1101/cshperspect.a037101.

29. Winkles JA. The TWEAK-Fn14 cytokine-receptor axis: discovery, biology and therapeutic targeting. Nat Rev Drug Discov. 2008;7(5):411–25. https://doi.org/10.1038/nrd2488.
30. Zoller V, Funcke JB, Keuper M, El Hay MA, Debatin KM, et al. TRAIL (TNF-related apoptosis-inducing ligand) inhibits human adipocyte differentiation via caspase-mediated downregulation of adipogenic transcription factors. Cell Death Dis. 2016;7(10):e2469. https://doi.org/10.1038/cddis.2016.286.
31. Anany MA, Kreckel J, Füllsack S, Rosenthal A, Otto C, et al. Soluble TNF-like weak inducer of apoptosis (TWEAK) enhances poly(I:C)-induced RIPK1-mediated necroptosis. Cell Death Dis. 2018;9(11):1084. https://doi.org/10.1038/s41419-018-1137-1.
32. Dorninger F, Forss-Petter S, Berger J. From peroxisomal disorders to common neurodegenerative diseases: the role of ether phospholipids in the nervous system. FEBS Lett. 2017;591(18):2761–78. https://doi.org/10.1002/1873-3468.12788.
33. Perez MA, Clostio AJ, Houston IR, Ruiz J, Magtanong L, et al. Ether lipid deficiency disrupts lipid homeostasis leading to ferroptosis sensitivity. PLoS Genet. 2022;18(9):e1010436. https://doi.org/10.1371/journal.pgen.1010436.
34. Calzada E, Onguka O, Claypool SM. Phosphatidylethanolamine metabolism in health and disease. Int Rev Cell Mol Biol. 2016;321:29–88. https://doi.org/10.1016/bs.ircmb.2015.10.001.
35. Jiang XC, Li Z. Sphingolipids and cholesterol. Adv Exp Med Biol. 2022;1372:1–14. https://doi.org/10.1007/978-981-19-0394-6_1.
36. Hammad SM, Lopes-Virella MF. Circulating sphingolipids in insulin resistance, diabetes and associated complications. Int J Mol Sci. 2023;24(18):14015. https://doi.org/10.3390/ijms241814015.
37. Houben T, Oligschlaeger Y, Hendrikx T, Bitorina AV, Walenbergh SMA, Van Gorp PJ, et al. Cathepsin D regulates lipid metabolism in murine steatohepatitis. Sci Rep. 2017;7:3494. https://doi.org/10.1038/s41598-017-03796-5.
38. Cabrera-Reyes F, Parra-Ruiz C, Yuseff MI, Zanlungo S. Alterations in lysosome homeostasis in lipid-related disorders: impact on metabolic tissues and immune cells. Front Cell Dev Biol. 2021;9:790568. https://doi.org/10.3389/fcell.2021.790568.
39. Fonteh AN, Samet JM, Chilton FH. Regulation of arachidonic acid, eicosanoid, and phospholipase A2 levels in murine mast cells by recombinant stem cell factor. J Clin Invest. 1995;96(3):1432–9. https://doi.org/10.1172/JCI118179.
40. Liu W, Zhu M, Gong M, Zheng W, Zeng X, Zheng Q, et al. Comparison of the effects of monounsaturated fatty acids and polyunsaturated fatty acids on liver lipid disorders in obese mice. Nutrients. 2023;15(14):3200. https://doi.org/10.3390/nu15143200.
41. Ravaut G, Légiot A, Bergeron KF, Mounier C. Monounsaturated fatty acids in obesity-related inflammation. Int J Mol Sci. 2021;22(1):330. https://doi.org/10.3390/ijms22010330.

Publisher's Note